Ivan Mironyuk[1], Nazarii Danyliuk[2], Liliia Turovska[3], Ihor Mykytyn[1], Volodymyr Kotsyubynsky[4]

# Structural, morphological and photocatalytic properties of nanostructured TiO₂/AgI photocatalyst

*[1]Department of Chemistry, Vasyl Stefanyk Precarpathian National University, Ivano-Frankivsk, Ukraine, myrif555@gmail.com*
*[2]Educational and Scientific Center of Material Science and Nanotechnology, Vasyl Stefanyk Precarpathian National University, Ivano-Frankivsk, Ukraine, danyliuk.nazariy@gmail.com*
*[3]Department of Medical Informatics, Medical and Biological Physics, Ivano-Frankivsk National Medical University, Ivano-Frankivsk, Ukraine, lturovska@ifnmu.edu.ua*
*[4]Department of Materials Science and New Technologies, Vasyl Stefanyk Precarpathian National University, Ivano-Frankivsk, Ukraine, kotsuybynsky@gmail.com*

Nanostructured TiO₂/AgI photocatalyst under the action of ultraviolet or visible electromagnetic radiation effectively neutralizes organic pollutants in the aqueous environment. It is a nanostructure in which micro- and small mesopores of anatase TiO₂ are filled with silver iodide in the superionic state. The content of the α-AgI ion-conducting phase in the volume of TiO₂ pores can be ~20 wt %.

To obtain a photocatalyst, titanium dioxide is synthesized by the sol-gel method, using a titanium aquacomplex solution $[Ti(OH_2)_6]^{3+} \cdot 3Cl^-$ and a $Na_2CO_3$ modifier additive as a precursor. The modifying additive during synthesis ensures the fixation of $=O_2CO$ carbonate groups on the surface of oxide material particles. The presence of these groups leads to an increase in both the pore volume and the specific surface area of TiO₂. The specific surface area of carbonized titanium dioxide is 368 $m^2 \cdot g^{-1}$, the pore volume is 0.28 $cm^3 \cdot g^{-1}$, and their size is 0.9-4.5 nm.

To fill the micro- and small mesopores of TiO₂ with the superionic α-AgI phase, $Ag^+$ cations are first adsorbed from the $AgNO_3$ solution on the titanium dioxide surface, and then the oxide material is contacted with the KI solution.

Compared to the Evonik P25-TiO₂ photocatalyst, the nanostructured TiO₂/AgI photocatalyst demonstrates a significantly higher efficiency of photodegradation of organic dyes Congo Red and Methyl Orange in visible and ultraviolet radiation. The most active TiO₂/40AgI sample achieved complete degradation of the CR dye (5 mg/L) in 6 minutes of UV irradiation ($\lambda = 365$ nm), while the efficiency of commercial P25-TiO₂ over the same time was only 42%.

**Keywords:** titania, Congo Red, Methyl Orange, photocatalyst.

## Introduction

To improve the spatial separation of photogenerated charges and increase the quantum yield of photocatalytic transformations, nanostructured binary photocatalysts are used. The coordinated energy of the conduction band and the valence band of these nanostructures contributes to the irreversible interfacial transfer of photogenerated electrons and holes.

In binary photocatalysts based on TiO₂, metal oxide [1–4] or chalcogenide semiconductors [5–7], conductive polymers [8–10], carbon materials such as graphite, fullerenes, graphene [11–14], etc. can perform the co-catalyst function.

The components of photocatalysts based on TiO₂ are also solid-state electrolytes, in particular, silver halides [15–17]. TiO₂/AgBr nanostructures have a photocatalytic effect in dye oxidation reactions, they are characterized by photobactericidal properties.

TiO$_2$-AgI nanocomposites obtained by mixing the corresponding sols exhibit photocatalytic activity in the reduction reactions of methylviologen [17].

TiO$_2$/AgI nanoheterostructures should be more efficient photocatalysts than nanocomposites of this composition. By definition, in a nanostructured photocatalyst, nanometer-scale components must be interconnected and placed in a certain order relative to each other. The large area of phase contact in these nanostructures and the ionic conductivity of AgI ensure the removal of photogenerated holes of the valence band of titanium dioxide and prevent their recombination with the electrons of the conduction band.

In this work, our goal was to synthesize a nanoheterostructural photocatalyst in which TiO$_2$ is combined with silver iodide in the superionic state, to study the structural and morphological characteristics of the photocatalyst, and to study its activity in dye oxidation reactions in ultraviolet and visible electromagnetic radiation.

# I. Experimental

## 1.1. Preparation of TiO$_2$/AgI nanostructures

Nanostructured TiO$_2$/AgI photocatalyst was obtained by filling titanium dioxide mesopores with silver iodide during the reaction between AgNO$_3$ and KI. Ag$^+$ cations were adsorbed from the AgNO$_3$ solution on the surface of the oxide material for AgI to enter the TiO$_2$ pores, and only then the oxide material was brought into contact with the KI solution. Due to the high Laplace pressure, AgI nanoparticles in the pores of the oxide material pass from the dielectric state (β-AgI phase) to the superionic state (α-AgI phase). The ionic conductivity of the α-AgI phase is $10^8$ times higher than the ionic conductivity of the β-AgI phase.

The synthesis of anatase nanoparticle TiO$_2$ is based on the sol-gel method, in which a solution of the [Ti(OH$_2$)$_6$]$^{3+}$·3Cl$^-$ aquacomplex is used as a precursor. In order to increase the pore volume of TiO$_2$, its specific surface area, and adsorption activity with respect to metal cations on the surface of the oxide material, carbonate groups =O$_2$CO were grafted during synthesis [18]. To implement this process, the modifying reagent Na$_2$CO$_3$ was introduced into the titanium precursor solution. Its percentage was 8 wt.% relative to TiO$_2$.

The mixture of reagents was diluted with water and kept at a temperature of 70°C for 30-40 minutes. After heating, the pH of the reaction medium was adjusted to 6-7 with a 10% NaOH solution. The resulting TiO$_2$ particles were removed from the reaction medium using a vacuum filter, then washed from adsorbed Na$^+$ and Cl$^-$ ions with distilled water and dried at a temperature of 120-140°C.

With a pore size of 0.9-4.5 nm and a pore volume of 0.28 cm$^3$·g$^{-1}$, the specific surface area of the synthesized TiO$_2$ was 370 m$^2$·g$^{-1}$.

Table 1 shows the morphological characteristics (specific surface area, pore volume) of base and modified TiO$_2$. The base titanium dioxide in the table is designated α-TiO$_2$, and the modified one is 8C-TiO$_2$. Morphological characteristics indicate that the modified TiO$_2$ exceeds the base one in terms of specific surface area and pore volume. The carbonated TiO$_2$ obtained by this method is an effective adsorbent for the extraction of metal cations from an aqueous medium.

To obtain nanoheterostructured photocatalysts, silver cations Ag$^+$ were adsorbed on the 8C-TiO$_2$ surface. To do this, an adsorbent was introduced into the AgNO$_3$ solution and kept for 30-40 minutes. It was removed from the dispersion medium and mixed with the KI solution. After 10-20 minutes of contact, the precipitate of the solid product was separated from the reaction medium, washed with distilled water, and dried at a temperature of 140-150$^0$C for 2 hours.

Studies of the adsorption of silver cations by carbonized TiO$_2$ showed that 1 g of the 8C-TiO$_2$ adsorbent extracts 190-210 mg of silver ions from an AgNO$_3$ solution.

To optimize the phase composition of the photocatalyst in the specified way, three test samples of the photocatalyst containing 20, 30, and 40 wt.% of silver iodide were obtained. These samples are designated TiO$_2$/20AgI, TiO$_2$/30AgI, and TiO$_2$/40AgI, respectively.

## 1.2. Characteristics of methods

Phase analysis of the TiO$_2$ samples and TiO$_2$/AgI nanostructures was carried out on an XRD-7000 Shimadzu X-ray diffractometer in copper anode radiation. Crystal phases were identified using the Mateh 3.0 software.

The morphological characteristics of powder materials, namely, their specific surface area, pore volume, and pore size distribution, were calculated from N$_2$ adsorption/desorption isotherms. Adsorption was studied at the boiling point of liquid nitrogen (T = 77 K) on an automatic sorbometer Quantachrome Autosorb (Nova 2200 e). Before radiation, the test samples were calcined in vacuum at a temperature of 180$^0$C for 24 hours. The pore size distribution was calculated using the density functional theory [19].

Images of TiO$_2$ particles and TiO$_2$/AgI nanostructures

**Table 1.**

Morphological characteristics of test samples (average value of specific surface area and pore volume)

| Test samples | Porous structure parameters | | | | | | | |
|---|---|---|---|---|---|---|---|---|
| | S, m$^2$·g$^{-1}$ | S$_{micro}$ m$^2$·g$^{-1}$ | S$_{meso}$ m$^2$·g$^{-1}$ | S$_{meso}$/S, % | V cm$^3$·g$^{-1}$ | V$_{micro}$ cm$^3$·g$^{-1}$ | V$_{meso}$ cm$^3$·g$^{-1}$ | V$_{meso}$/V, % |
| a-TiO$_2$ | 239 | 100 | 139 | 58 | 0.15 | 0.054 | 0.098 | 64.4 |
| 8C-TiO$_2$ | 370 | 6 | 364 | 98 | 0.28 | 0.001 | 0.279 | 99.6 |
| TiO$_2$/40AgI | 222 | - | 222 | 100 | 0.20 | - | 0.20 | 100 |

Ivan Mironyuk, Nazarii Danyliuk, Liliia Turovska, Ihor Mykytyn, Volodymyr Kotsyubynsky

were obtained using a JSM-2100F transmission electron microscope and a REMMA-102 scanning electron microscope. The scanning electron microscope is connected to an energy-dispersive X-ray spectrometer. This allowed us to control the elemental composition of the test samples.

### 1.3. Evaluation of photocatalytic performance

The photocatalytic activity of nanostructured TiO$_2$/AgI composites was evaluated by studying the photodegradation of dye solutions: Congo Red (CR) and Methyl Orange (MO) under the influence of UV and visible electromagnetic radiation. The source of electromagnetic radiation was LEDs with a wavelength of 365, 395 and 430 nm. The power of each LED was 5 W. The design of the photoreactor is described in detail in [20].

Before the start of the experiment, a suspension containing 30 mg of photocatalyst and 20 ml of an aqueous solution of CR or MO dye (5 mg/L) was stirred with a magnetic stirrer for 30 minutes in the dark to ensure the establishment of an adsorption-desorption equilibrium between the dye molecules and the photocatalyst surface at room temperature. After that, the suspension with its continuous stirring was irradiated with electromagnetic radiation with a given wavelength. The photodegradation kinetics of the dyes was recorded with a DT-1309 light meter. The final concentration of the dye in the solution was determined with a Ulab 102UV spectrophotometer. A detailed description of this technique and calibration

dependences are given in [21]. The percentage of dye degradation was determined by equation (1):

$$\% \text{ degradation dye} = C_0\text{-}C/C_0 \cdot 100\%, \qquad (1)$$

where % degradation dye is the percentage of dye degradation, $C_0$ is its initial concentration, and $C$ is the dye concentration at time t. A commercial P25-TiO$_2$ photocatalyst from Evonik was also studied under these conditions.

## II. Results and discussion

### 2.1. Morphological condition of the samples

The liquid-phase method for obtaining carbonated TiO$_2$ makes it possible to obtain an oxide material with small mesopores and their large total volume (Table 1). The image of the microstructure of the 8C-TiO$_2$ sample with a resolution of 5 nm (Fig. 1a) makes it possible to see the primary particles of the oxide material, which are anatase nanocrystallites. Their size is 3-7 nm, and they have a faceted shape. Rows of TiO$_6$ octahedra are visible on the faces of individual crystallites. White dots in the rows indicate the absence of titanium atoms in them. Defects in the structure of crystallites are micropores < 1.5 nm in size.

During the sol-gel synthesis, the primary particles-crystallites are combined into aggregates. The aggregate
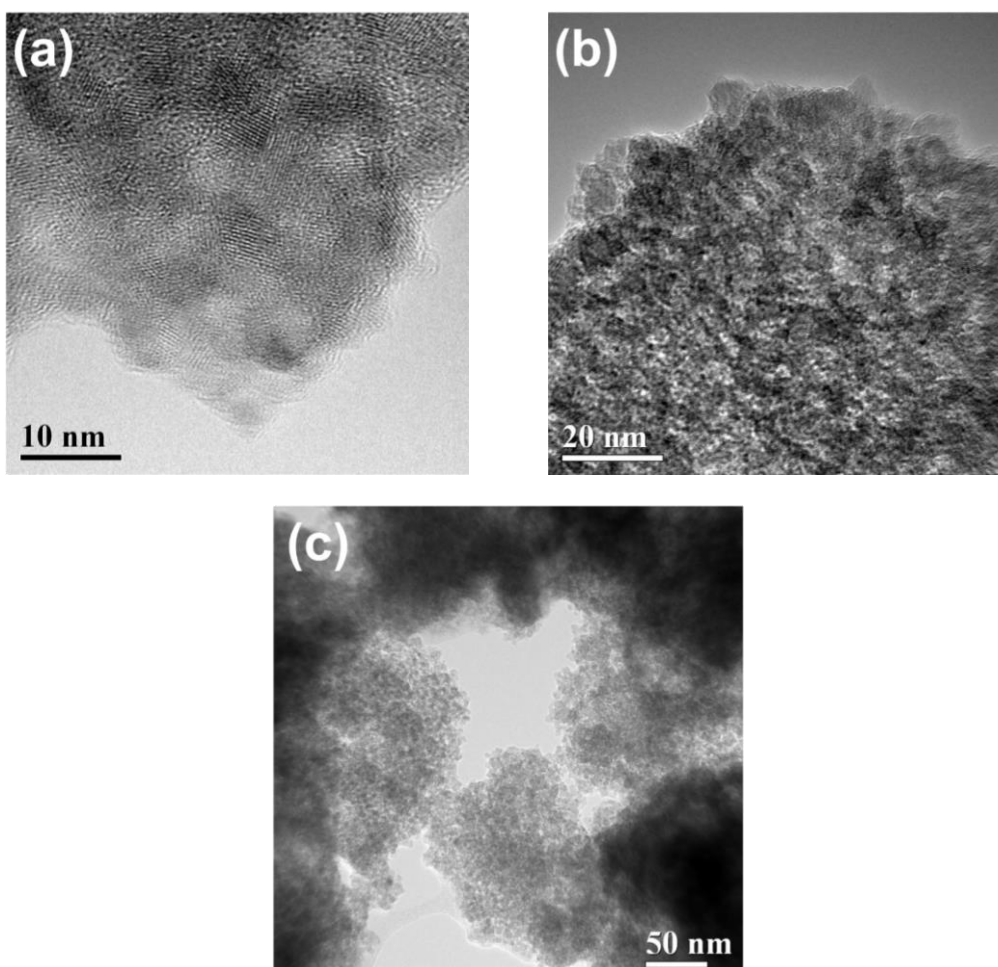


**Fig. 1.** Image of primary particles (a) and their aggregates (b, c) in the 8C-TiO$_2$ sample.

size is 180-360 nm (Fig. 1c). The image of the aggregate with a resolution of 20 nm (Fig. 1b) shows numerous white areas 1-4 nm in size, which are mesopores.

Filling the pore volume of carbonated $TiO_2$ with silver iodide leads to a decrease in its specific surface area and pore volume. Thus, the specific surface area of the $TiO_2$/40AgI test sample is 222 $m^2 \cdot g^{-1}$, and that of the 8C-$TiO_2$ sample is 370 $m^2 \cdot g^{-1}$ (Table 1). The pore volume of this nanostructured material decreases from 0.28 $cm^2 \cdot g^{-1}$ to 0.2 $cm^2 \cdot g^{-1}$ compared to carbonated $TiO_2$. The contact area between titanium dioxide and the α-AgI phase is 148 $m^2 \cdot g^{-1}$. An analysis of the pore size distribution in carbonated $TiO_2$ and in the $TiO_2$/40AgI sample shows (Fig. 3) that silver iodide in the nanostructured material is localized only in small mesopores 2.4-3.2 nm in size and micropores, and these pores are half filled with AgI. The absence of silver iodide in pores with a diameter of 3.2-4.5 nm is due to the fact that during the AgI formation reaction, pressure arises that displaces reaction products from the volume of these pores, so the condensation of silver iodide molecules occurs outside the pore volume of the oxide material. The formation of AgI crystallites in the volume of small mesopores and micropores is probably due to their small necks, which limit the extraction of AgI molecules from their volume.
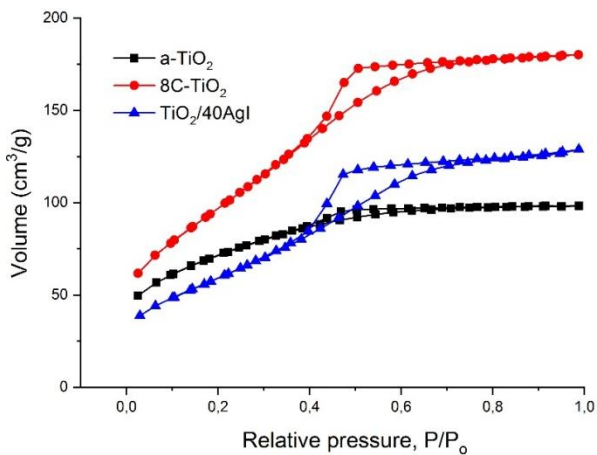


**Fig. 2.** Isotherms of adsorption/desorption of N₂ molecules by test samples.
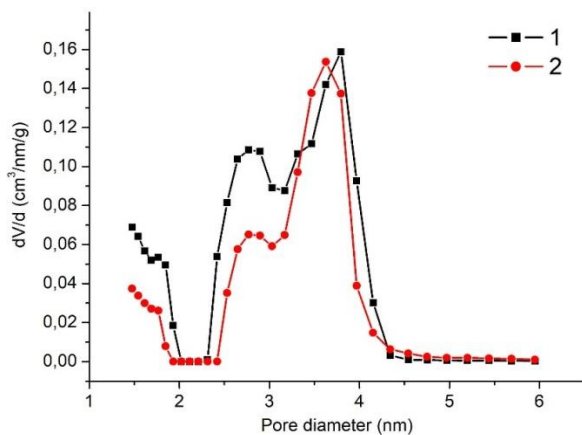


**Fig. 3.** Pore size distribution in carbonated titanium dioxide 8C-$TiO_2$ (1) and photocatalyst $TiO_2$/40AgI (2).

Fig. 4 shows an image of $TiO_2$/40AgI sample particles obtained using a scanning electron microscope. We can see that the mixture with large xerogel-like particles of $TiO_2$/40AgI of black color contains small particles of AgI of white color. The elemental composition of $TiO_2$/AgI and AgI particles is confirmed by the spectra of energy-dispersive X-ray microanalysis (Fig. 5 a, b).
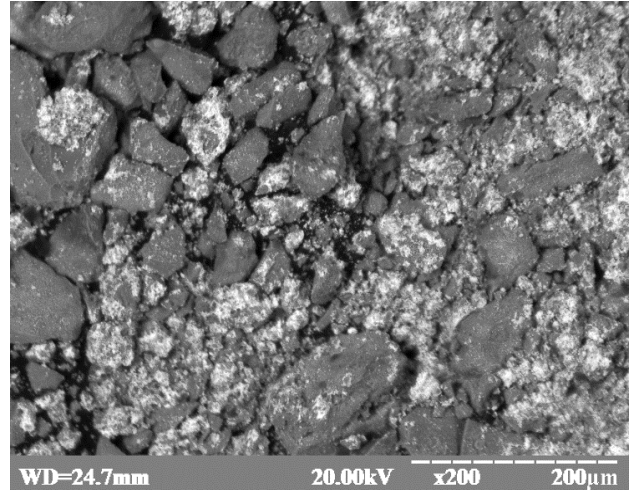


**Fig. 4.** Image of $TiO_2$/40AgI particles. Black particles are $TiO_2$/AgI heterostructure xerogel, white particles are AgI.

## 2.2. Phase composition of the photocatalyst

Silver iodide belongs to the class of solid electrolytes, which are characterized by ionic conductivity. At room temperature and normal pressure, the crystalline state of silver iodide corresponds to the β-AgI phase [22]. In some cases, a metastable γ-AgI phase may also be present along with this phase.

At normal pressure, according to the phase diagram [22] (Fig. 6), at a temperature of 146⁰C, the β-AgI phase undergoes phase transition into the α-AgI phase. As a result of this phase transition, AgI passes from the dielectric to the superionic state. In the superionic state, the electrical conductivity L of the α-AgI phase is 1.38 S·cm⁻¹ [22]. This value is close to the L value of concentrated liquid electrolytes. At room temperature, the electrical conductivity of the β-AgI phase is 10⁻⁸ S·cm⁻¹.

The phase diagram of AgI indicates that with increasing pressure, the temperature of the β→α-phase transition decreases. At a pressure of 270 MPa, AgI acquires a superionic state already at room temperature. It is important to note that the temperature of AgI transition to the superionic state depends on the particle size. Very small nanocrystallites in the superionic state can exist at room temperature. This phenomenon is due to the action of Laplace pressure. Phenomenologically, the Laplace pressure $P_L$ arises due to the action of surface tension σ and its value depends on the curvature of the surface of the solid. For spherical particles

$$P_L = \frac{4\sigma}{d} \qquad (2),$$

where $d$ is the effective particle diameter.

Ivan Mironyuk, Nazarii Danyliuk, Liliia Turovska, Ihor Mykytyn, Volodymyr Kotsyubynsky
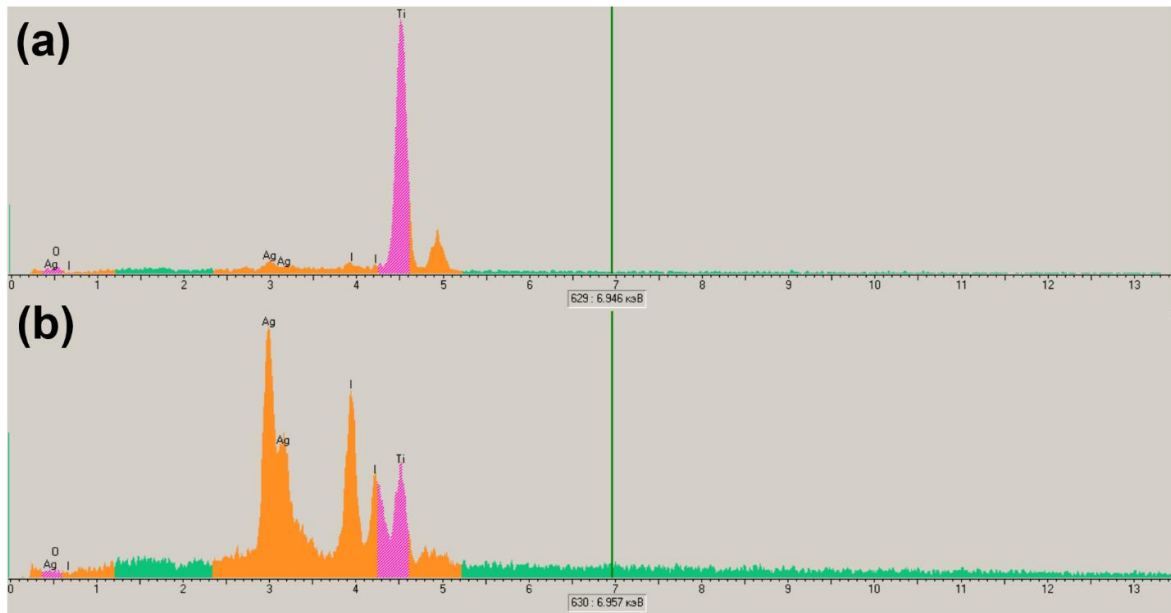


**Fig. 5.** Energy-dispersive spectra of TiO₂/AgI heterostructure particles (a) and AgI particles (b) of the TiO₂/40AgI test sample.
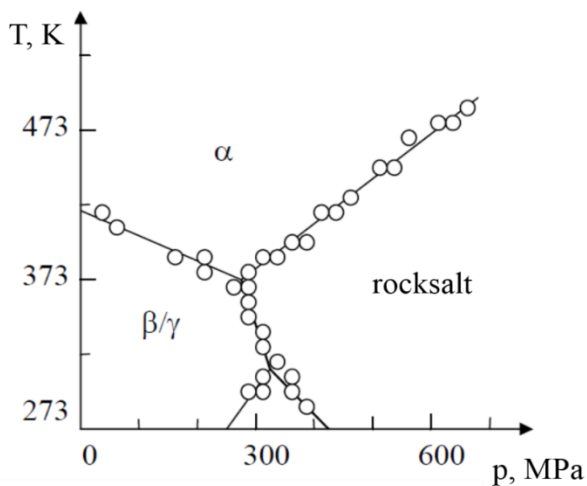


**Fig. 6.** Phase diagram of AgI.

The calculation shows that silver iodide particles in pores of the photocatalyst with a diameter of 2.4 nm at an AgI surface tension of 0.18 J·m⁻² are under pressure of 300 MPa. At this pressure, AgI particles localized in small titanium dioxide mesopores pass into the superionic state.

Phase analysis of the test samples of TiO₂/20AgI, TiO₂/30AgI and TiO₂/40AgI by X-ray diffractometry revealed an anatase modification of TiO₂ and two phases of silver iodide – α-AgI and β-AgI in each sample. The diffraction patterns of the test samples are shown in Fig. 7.

Table 2 shows the space symmetry groups of the phases, their content and lattice parameters. The α-AgI phase is localized in small mesopores and micropores of anatase, while the β-AgI phase is located outside the pore volume of TiO₂. It can be seen from the presented data that with an increase in the content of silver iodide in the samples from 20% to 40%, the content of the α-AgI phase in the pores of the oxide material increases from 6.17 wt.% to 20.17 wt.%. Characteristically, with an increase in the

content of the current-conducting phase, the efficiency of the nanostructured photocatalyst increases.
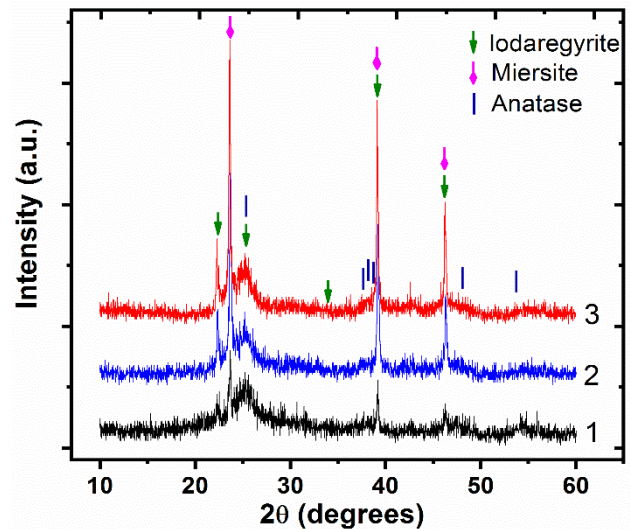


**Fig. 7.** X-ray diffraction patterns of TiO₂/20AgI (1), TiO₂/30AgI (2), and TiO₂/40AgI (3) samples.

### 2.3. Discussion of the results
#### 2.3.1 Effect of AgI loading percentage

AgI effectively absorbs in the visible light region [23], so the percentage of AgI incorporation into titanium dioxide pores should have a significant effect on the activity of nanostructured photocatalysts. The photocatalytic activity of AgI/TiO₂ photocatalysts was evaluated by their ability to affect the degradation of dyes under the action of UV and visible electromagnetic radiation. Figs. 8-11 show that the efficiency of destruction of molecules of CR and MO dyes increases with an increase in the percentage of AgI in the nanostructured photocatalyst. The maximum efficiency of CR and MO removal is achieved in the TiO₂/40% AgI photocatalyst.

**Table 2.**

Phase composition of samples and lattice parameters of anatase TiO₂, α-AgI and β-AgI.

| Sample | TiO₂ (Anatase) ICSD # 44882 Tetragonal, I41/amd | | | $\beta-$AgI (Iodaregyrite) ICSD # 65063 Hexagonal, P6mm | | | $\alpha-$AgI (Miersite) ICSD # 52361 Cubic, F-4 3m | |
|---|---|---|---|---|---|---|---|---|
| | Content, % | a, Å | c, Å | Content, % | a, Å | c, Å | Content, % | a, Å |
| TiO₂/40AgI | 60.0± 4.4 | 3.7839± 0.0024 | 9.4432± 0.0089 | 19.83± 7.73 | 4.5651± 0.0679 | 7.5191± 0.2779 | 20.17± 0.61 | 6.4914± 0.0035 |
| TiO₂/30AgI | 70.0± 4.11 | 3.7365± 0.0046 | 9.39322 0.05712 | 19.26± 0.48 | 4.5765± 0.0030 | 7.4828± 0.0108 | 10.74± 0.39 | 6.4889± 0.0017 |
| TiO₂/20AgI | 80.0± 3.29 | 3.7752± 0.0034 | 9.4015± 0.01634 | 13.83± 0.51 | 4.5687± 0.0016 | 7.4782± 0.0091 | 6.17± 0.73 | 6.4924± 0.00132 |

As shown in Figs. 8-11, the CR and MO dyes were effectively degraded as a result of the action of test samples of photocatalysts. Accordingly, with an increase in the mass fraction of AgI from 20% to 40%, the efficiency of dye degradation increases, while the reaction rate constants increase from 0.1277 min⁻¹ to 0.1844 min⁻¹ for CR and from 0.0640 min⁻¹ to 0.1051 min⁻¹ for MO when irradiated with visible light ($\lambda$= 430 nm). The photocatalytic reaction occurs on the surface of the catalyst; therefore, the adsorption capacity of the 8C-TiO₂ base has a significant effect on the rate of degradation of the CR and MO dyes.

It is known that the combination of AgI and TiO₂ leads to a shift of the absorption spectra to the visible light region [24]. AgI nanoparticles act as a sensitizer [25]. Accordingly, the nanostructured TiO₂/AgI composite efficiently absorbs visible light during photocatalytic reactions. The obtained samples of photocatalysts were studied at wavelengths of electromagnetic radiation of 365, 395, and 430 nm. Among all the samples, the TiO₂/40AgI photocatalyst at an irradiation wavelength of 365 nm destroyed the CR and MO dyes four times faster than the P25-TiO₂ photocatalyst.

**2.3.2 Photocatalytic degradation of Congo Red**

The kinetics of photodegradation of Congo Red by test samples of the photocatalyst is shown in Fig. 8. The obtained kinetic curves are described by a pseudo-first order equation, since the function of dependence of ln(C/C₀) on the reaction time (t) shows linearity with high correlation coefficients in the range from 0.9016 to 0.9983 (Table 3), where C₀ is the initial concentration of CR before irradiation, C is the concentration of CR at reaction time t, k is the reaction rate constant. The calculated photodegradation rate constants of Congo Red are shown in Fig. 9. Self-photodegradation of CR dye under irradiation with LEDs is not observed. The efficiency of the degradation of Congo Red for all samples decreases with increasing irradiation wavelength from 365 to 430 nm. For the TiO₂/40AgI sample, the reaction rate constants are 0.4099 min⁻¹ and 0.1844 min⁻¹, respectively.

In particular, the incorporation of AgI into TiO₂ mesopores contributes to an increase in the activity of the photocatalyst in the visible light spectrum. The TiO₂/40AgI sample during irradiation at a wavelength of 430 nm showed almost 5 times higher efficiency
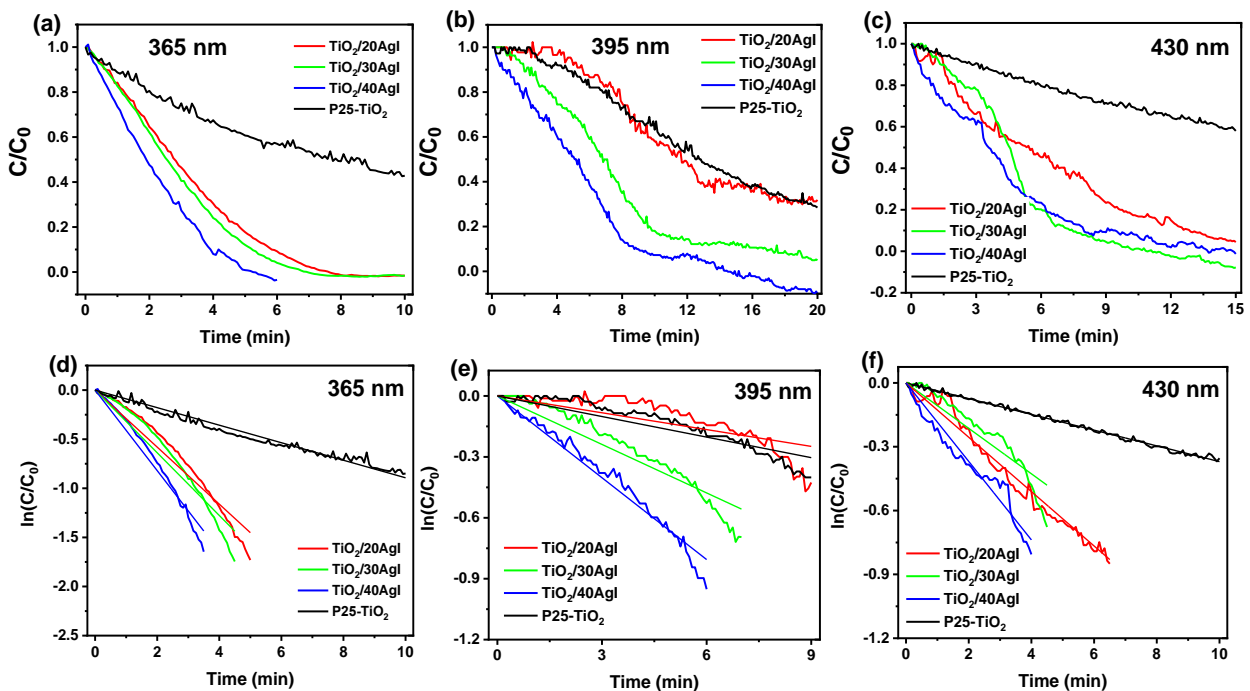


**Fig. 8.** (a-c) Effect of AgI concentration on CR dye degradation; (d-f) experimental lines transformed according to first-order kinetics.

**Table 3.**
Rate constants of the first order kinetic model of CR photodegradation on $TiO_2/AgI$ and $P25-TiO_2$ samples
(experimental conditions: solution volume 20 ml, dye concentration 5 mg/L).

| λ, nm | $TiO_2/20AgI$ | | $TiO_2/30AgI$ | | $TiO_2/40AgI$ | | $P25-TiO_2$ | |
|---|---|---|---|---|---|---|---|---|
| | k, min$^{-1}$ | $R^2$ | k, min$^{-1}$ | $R^2$ | k, min$^{-1}$ | $R^2$ | k, min$^{-1}$ | $R^2$ |
| 365 | 0.2903 | 0.9794 | 0.3191 | 0.9753 | 0.4099 | 0.9885 | 0.0892 | 0.9933 |
| 395 | 0.0275 | 0.9016 | 0.0795 | 0.9631 | 0.1342 | 0.9901 | 0.0337 | 0.9362 |
| 430 | 0.1277 | 0.9881 | 0.1068 | 0.9462 | 0.1844 | 0.9843 | 0.0369 | 0.9983 |
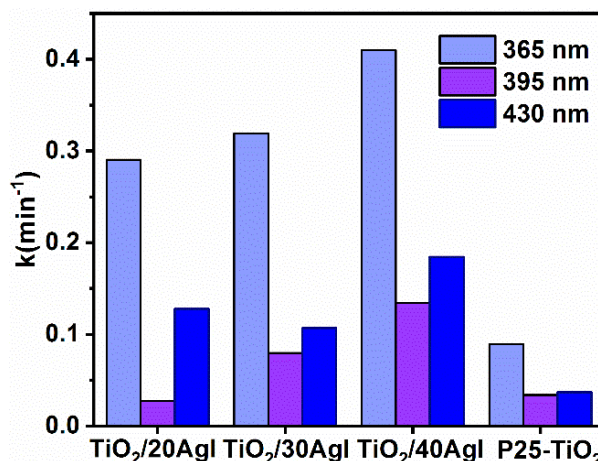


**Fig. 9.** Rate constants of the first-order kinetic model of CR dye photodegradation on $TiO_2/20AgI$, $TiO_2/30AgI$, $TiO_2/40AgI$, and $P25-TiO_2$ samples.

compared to $P25-TiO_2$ with reaction rate constants of 0.1844 min$^{-1}$ and 0.0369 min$^{-1}$, respectively. Test samples show increased photocatalytic activity when illuminated with visible light (430 nm) for 15 minutes. In the photodegradation of CR dye by $TiO_2/20AgI$, $TiO_2/30AgI$, and $TiO_2/40AgI$ samples when irradiated with a wavelength of 365 nm and 430 nm, the efficiency is 96%, 100%, and 100%, respectively. The resulting nanostructured $TiO_2/AgI$ composites showed better efficiency when irradiated with 365 nm light compared to commercial $P25-TiO_2$. For example, the $TiO_2/40AgI$ sample achieved complete degradation of CR in 6 minutes of irradiation, while $P25-TiO_2$ destroyed the dye by only 42% during the same period of time. According to the efficiency of CR photodegradation, test samples can be arranged as follows:
$P25-TiO_2$ < $TiO_2/20AgI$ < $TiO_2/30AgI$ < $TiO_2/40AgI$. Thus, at 40% AgI, the photocatalytic activity was the highest. A further increase in the content of AgI in a nanostructured composite is unreasonable since it entails electron-hole recombination [26]. A similar result was described in [24]. The $0.2Ag@AgI/TiO_2$ photocatalyst showed the highest efficiency of RhB removal (91%) in 90 min. As the content of AgI increases, its activity decreases.

**2.3.3 Photocatalytic degradation of Methyl Orange**
To illustrate that the resulting $TiO_2/AgI$ nanostructures can degrade various organic toxicants, their photocatalytic activity was measured by monitoring the decomposition of Methyl Orange dye in aqueous solution under the same conditions as Congo Red. Changes in the MO concentration during the experiments were recorded using a DT-1309 light meter. The color of MO gradually decreases and the color of the solution changes from orange to colorless within 20 minutes of the

reaction, indicating that the chromophore groups of the MO molecules are destroyed, and the corresponding color change can be registered using a light meter. For comparison, similar MO photodegradation experiments were carried out in the presence of commercial $P25-TiO_2$. The efficiency of MO photodegradation in 10 min of photooxidation at a wavelength of 365 nm reaches 95%, 100%, 100%, and 59% for $TiO_2/20AgI$, $TiO_2/30AgI$, $TiO_2/40AgI$, and $P25-TiO_2$ samples, respectively. The efficiency of MO degradation in 20 min of the irradiation reaction at a wavelength of 395 nm is 99%, 100%, 100%, and 74% for $TiO_2/20AgI$, $TiO_2/30AgI$, $TiO_2/40AgI$, and $P25-TiO_2$ samples, respectively. The efficiency of MO degradation in 20 min of 430 nm light irradiation is 67%, 84%, 99%, and 44% for $TiO_2/20AgI$, $TiO_2/30AgI$, $TiO_2/40AgI$, and $P25-TiO_2$ samples, respectively. The $TiO_2/40AgI$ sample showed the highest photocatalytic activity among the test samples. According to the efficiency of MO degradation, the samples can be arranged as follows:
$P25-TiO_2$ < $TiO_2/20AgI$ < $TiO_2/30AgI$ < $TiO_2/40AgI$.
The photocatalytic degradation of MO is described by a first order equation (Fig. 10), as is the photodegradation of most organic substances [20,27,28]. Linear transformations of kinetic curves are shown in Figs. 10 d-f in the coordinates of $ln(C/C_0)$ versus reaction time t. The reaction rate constants of MO photodegradation for various photocatalysts $TiO_2/20AgI$, $TiO_2/30AgI$, $TiO_2/40AgI$, and $P25-TiO_2$ are shown in Fig. 11. The value of k for the process of MO photodegradation by $TiO_2/40AgI$ photocatalyst was the highest compared to other samples. The reaction rate constant was 0.3698 min$^{-1}$, 0.1885 min$^{-1}$, 0.1051 min$^{-1}$ for light energy sources with wavelengths of 365, 395, and 430 nm, respectively. It was determined that the photocatalytic activity of $TiO_2/40AgI$ significantly exceeds the activity of $P25-TiO_2$, especially

380
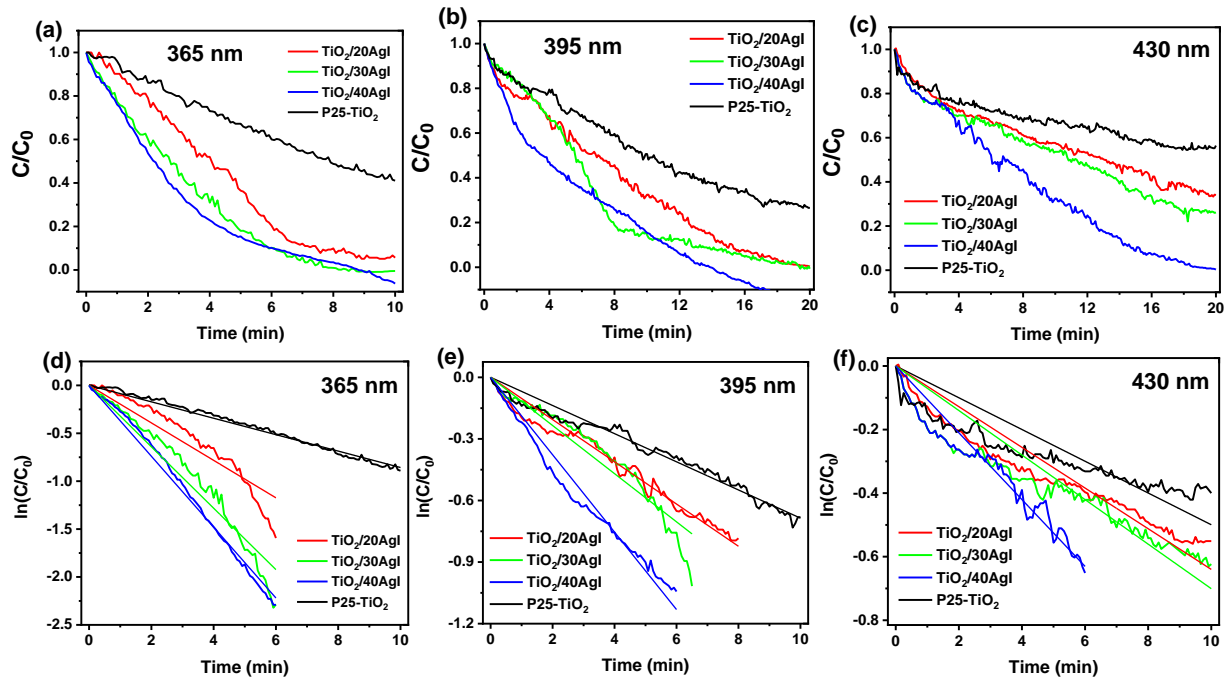
**Fig. 10.** (a-c) Effect of AgI concentration on MO dye degradation; (d-f) experimental lines transformed according to first-order kinetics.

**Table 4.**

Rate constants of the first order kinetic model of MO photodegradation on the TiO$_2$ sample (experimental conditions: solution volume 20 ml, dye concentration 5 mg/L).

| λ, nm | TiO$_2$/20AgI | | TiO$_2$/30AgI | | TiO$_2$/40AgI | | P25-TiO$_2$ | |
|---|---|---|---|---|---|---|---|---|
| | k, min$^{-1}$ | $R^2$ | k, min$^{-1}$ | $R^2$ | k, min$^{-1}$ | $R^2$ | k, min$^{-1}$ | $R^2$ |
| **365** | 0.1956 | 0.9578 | 0.3204 | 0.9826 | 0.3698 | 0.9963 | 0.0857 | 0.9965 |
| **395** | 0.1028 | 0.9917 | 0.1173 | 0.9757 | 0.1885 | 0.9931 | 0.0685 | 0.9928 |
| **430** | 0.0640 | 0.9786 | 0.0700 | 0.9687 | 0.1051 | 0.9838 | 0.0499 | 0.9457 |
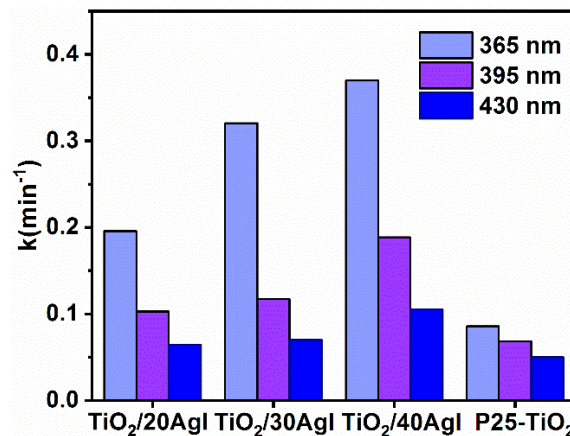


**Fig. 11.** Rate constants of the first-order kinetic model of MO dye photodegradation on TiO$_2$/20AgI, TiO$_2$/30AgI, TiO$_2$/40AgI, and P25-TiO$_2$ samples.

when irradiated at a wavelength of 430 nm, the reaction rate constant is twice as high, which is explained by the presence of AgI nanoparticles in TiO$_2$ mesopores. Thus, the TiO$_2$/40AgI photocatalyst can provide effective degradation of MO under UV and visible light irradiation.

Table 5 shows the results of the efficiency of similar photocatalysts based on TiO$_2$ and AgI in the photodegradation of various organic dyes. Under optimized experimental conditions, the activity of the

resulting TiO$_2$/AgI nanostructures significantly exceeded the efficiency of the nanocomposites presented in Table 5. Thus, nanostructured TiO$_2$/AgI photocatalysts obtained by this method can be used to neutralize organic pollutants in an aqueous medium.

Efficient separation of electron-hole pairs in the nanostructured TiO$_2$/AgI composite increases its photocatalytic activity in photodegradation reactions of CR and MO dyes under UV and visible irradiation.

Ivan Mironyuk, Nazarii Danyliuk, Liliia Turovska, Ihor Mykytyn, Volodymyr Kotsyubynsky

Comparison of photoactivity of nanocomposites based on $TiO_2$ and AgI

| Photocatalyst | Light source | Experimental conditions | Photodegradation efficiency | Ref |
|---|---|---|---|---|
| 0.2Ag@AgI/TiO$_2$ | Xe (1000 W) | Catalyst = 50 mg<br>[RhB] = 10 mg/L | 91% in 90 min | [24] |
| 0.2-AgI–TiO$_2$ | Xe ($\lambda > 420$ nm) | Catalyst = 10 mg<br>[BDE209] = $1.0 \cdot 10^{-5}$ mol·L$^{-1}$ | 70% in 180 min | [27] |
| TiO$_2$ QDs/CDs/Ag | 50W LED | Catalyst = 100 mg<br>[RhB] = $1.0 \cdot 10^{-5}$ mol·L$^{-1}$ | 97% in 20 min | [25] |
| 30AgI@TiO$_2$/U6N | Hg lamp (500W, $\lambda > 400$ nm) | Catalyst = 20 mg<br>[RhB] = 20 mg/L | 100% in 30 min | [29] |
| Ag-AgI(4%)-TiO$_2$/CNFs | Xe (300 W) | Catalyst = 100 mg<br>[MO] = 10 mg/L | 97% in 180 min | [30] |
| AgI–TiO$_2$–cotton | Xe (1000 W) ($\lambda > 400$ nm) | [MO] = 5 mg/L | 56% in 120 min | [31] |
| AgI-TiO$_2$/PAN | Xe (300 W) | Catalyst = 200 mg<br>[MO] = 50 mg/L | 87.8% in 270 min | [32] |
| TiO$_2$/40AgI | 10 W LED ($\lambda = 430$ nm) | Catalyst = 30 mg<br>[CR] = 5 mg/L | 100% in 15 min | This work |
| TiO$_2$/40AgI | 10 W LED ($\lambda = 430$ nm) | Catalyst = 30 mg<br>[MO] = 5 mg/L | 100% in 20 min | This work |

## Conclusions

This paper describes the synthesis and properties of nanostructured TiO$_2$/AgI photocatalysts. Filling micro- and mesopores of TiO$_2$ with AgI nanoparticles in the superionic state is an effective strategy for obtaining photocatalysts efficient in ultraviolet and visible electromagnetic radiation. Synthesis of TiO$_2$ has been carried out by the sol-gel method using a solution of the titanium aquacomplex $[Ti(OH_2)_6]^{3+} \cdot 3Cl^-$ and a Na$_2$CO$_3$ additive-modifier as a precursor. The presence of carbonate groups $=O_2CO$ on the surface of TiO$_2$ leads to an increase in the pore volume and specific surface area of the photocatalyst. The specific surface area of carbonated titanium dioxide is 368 m$^2$·g$^{-1}$, the pore volume is 0.28 cm$^3$·g$^{-1}$, and their size is 0.9-4.5 nm. The process of filling micro- and small mesopores of TiO$_2$ with the superionic α-AgI phase consists in the adsorption of Ag$^+$ cations on the surface of titanium dioxide, followed by the interaction of the oxide material with the KI solution. Among the studied nanostructured composites, the TiO$_2$/40AgI sample was the most effective, destroying CR and MO dyes four times faster than commercial P25-TiO$_2$ under UV irradiation ($\lambda = 365$ nm). According to the photodegradation efficiency of CR and MO, the studied samples can be arranged as follows: P25-TiO$_2$<TiO$_2$/20AgI<TiO$_2$/30AgI<TiO$_2$/40AgI under UV and visible irradiation. The high efficiency of the nanostructured TiO$_2$/40AgI photocatalyst will make it possible to use it to neutralize toxic organic substances in the aqueous environment.

***Mironyuk Ivan*** – Doctor of Chemical Sciences, Head of the Department of Chemistry, Vasyl Stefanyk Precarpathian National University;
***Danyliuk Nazarii*** – PhD student, leading specialist at the Educational and Scientific Center of Material Science and Nanotechnology, Vasyl Stefanyk Precarpathian National University;
***Turovska Liliia*** – Associate Professor of the Department of Medical Informatics, Medical and Biological Physics, Ivano-Frankivsk National Medical University;
***Mykytyn Ihor*** – Associate Professor of the Chemistry Department, Vasyl Stefanyk Precarpathian National University;
***Kotsyubynsky Volodymyr*** – Doctor of Physical and Mathematical Sciences, Vasyl Stefanyk Precarpathian National University.

[1] M.K.I. Senevirathna, P.K.D.D.P. Pitigala, K. Tennakone, *Water photoreduction with Cu$_2$O quantum dots on TiO$_2$ nano-particles*, J. Photochem. Photobiol. A Chem. 171, 257 (2005); https://doi.org/10.1016/j.jphotochem.2004.10.018.
[2] D.L. Liao, C.A. Badour, B.Q. Liao, *Preparation of nanosized TiO$_2$/ZnO composite catalyst and its photocatalytic activity for degradation of methyl orange*, J. Photochem. Photobiol. A Chem. 19, 11 (2008); https://doi.org/10.1016/j.jphotochem.2007.07.008.
[3] L.C. Chen, F.R. Tsai, S.H. Fang, Y.C. Ho, *Properties of sol-gel SnO$_2$/TiO$_2$ electrodes and their photoelectrocatalytic activities under UV and visible light illumination*, Electrochim. Acta. 54, 1304 (2009); https://doi.org/10.1016/j.electacta.2008.09.009.

[4]  E. V. Skorb, L.I. Antonouskaya, N.A. Belyasova, D.G. Shchukin, H. Möhwald, D. V. Sviridov, *Antibacterial activity of thin-film photocatalysts based on metal-modified TiO₂ and TiO₂: In₂O₃ nanocomposite*, Appl. Catal. B Environ. 84, 94 (2008); https://doi.org/10.1016/j.apcatb.2008.03.007.

[5]  J.S. Jang, H.G. Kim, U.A. Joshi, J.W. Jang, J.S. Lee, *Fabrication of CdS nanowires decorated with TiO₂ nanoparticles for photocatalytic hydrogen production under visible light irradiation*, Int. J. Hydrogen Energy. 33; 5975 (2008); https://doi.org/10.1016/j.ijhydene.2008.07.105.

[6]  W. Ho, J.C. Yu, *Sonochemical synthesis and visible light photocatalytic behavior of CdSe and CdSe/TiO₂ nanoparticles*, J. Mol. Catal. A Chem. 247, 268 (2006); https://doi.org/10.1016/j.molcata.2005.11.057.

[7]  D. Jing, L. Guo, *WS₂ sensitized mesoporous TiO₂ for efficient photocatalytic hydrogen production from water under visible light irradiation*, Catal. Commun. 8, 795 (2007); https://doi.org/10.1016/j.catcom.2006.09.009.

[8]  G. Liao, S. Chen, X. Quan, Y. Zhang, H. Zhao, *Remarkable improvement of visible light photocatalysis with PANI modified core-shell mesoporous TiO₂ microspheres*, Appl. Catal. B Environ. 102, 126 (2011); https://doi.org/10.1016/j.apcatb.2010.11.033.

[9]  H.C. Liang, X.Z. Li, *Visible-induced photocatalytic reactivity of polymer-sensitized titania nanotube films*, Appl. Catal. B Environ. 86, 8 (2009); https://doi.org/10.1016/j.apcatb.2008.07.015.

[10]  D. Wang, Y. Wang, X. Li, Q. Luo, J. An, J. Yue, *Sunlight photocatalytic activity of polypyrrole-TiO₂ nanocomposites prepared by "in situ" method*, Catal. Commun. 9, 1162 (2008); https://doi.org/10.1016/j.catcom.2007.10.027.

[11]  J. Zhong, F. Chen, J. Zhang, *Carbon-Deposited TiO₂: Synthesis, Characterization, and Visible Photocatalytic Performance*, J. Phys. Chem. 933 (2010); https://doi.org/10.1021/jp909835m.

[12]  R. Sellappan, J. Zhu, H. Fredriksson, R.S. Martins, M. Zäch, D. Chakarov, *Preparation and characterization of TiO₂ / carbon composite thin films with enhanced photocatalytic activity,* J. Mol. Catal. A. Chem. 335, 136 (2011); https://doi.org/10.1016/j.molcata.2010.11.025.

[13]  S. Mu, Y. Long, S. Kang, J. Mu, *Surface modification of TiO₂ nanoparticles with a C 60 derivative and enhanced photocatalytic activity for the reduction of aqueous Cr (VI) ions*, Catal. Commun. 11, 741 (2010); https://doi.org/10.1016/j.catcom.2010.02.006.

[14]  T. Graphene, T. Different, Y. Zhang, Z. Tang, X. Fu, Y. Xu, *TiO₂-Graphene Nanocomposites for Gas-Phase Photocatalytic Degradation of Volatile Aromatic Pollutant: Is TiO₂-graphene truly different from other TiO₂-carbon composite materials*, ACS Nano. 4, 7303 (2010); https://doi.org/10.1021/nn1024219.

[15]  Y. Zang, R. Farnood, *Photocatalytic activity of AgBr/TiO₂ in water under simulated sunlight irradiation*, Appl. Catal. B. 79, 334 (2008); https://doi.org/10.1016/j.apcatb.2007.10.019.

[16]  J. Yu, G. Dai, B. Huang, *Fabrication and Characterization of Visible-Light-Driven Plasmonic Photocatalyst Ag/AgCl/TiO₂ Nanotube Arrays*, J. Phys. Chem. C., 16394 (2009); https://doi.org/10.1021/jp905247j.

[17]  D. Fitzmaurice, H. Frei, *Time-resolved optical study on the charge carrier dynamics in a TiO₂/AgI sandwich colloid*, J. Phys. Chem., 9176 (1995); https://doi.org/10.1021/j100022a034.

[18]  I. Mironyuk, T. Tatarchuk, M. Naushad, H. Vasylyeva, I. Mykytyn, *Highly efficient adsorption of strontium ions by carbonated mesoporous TiO₂*, J. Mol. Liq., 285, 742 (2019); https://doi.org/10.1016/J.MOLLIQ.2019.04.111.

[19]  V.M. Gun'ko, V.V. Turov, *Nuclear magnetic resonance studies of interfacial phenomena*, CRC Press. Boca Rat., (2013); https://doi.org/10.1201/b14202.

[20]  T. Tatarchuk, N. Danyliuk, A. Shyichuk, W. Macyk, M. Naushad, *Photocatalytic degradation of dyes using rutile TiO₂ synthesized by reverse micelle and low temperature methods: real-time monitoring of the degradation kinetics*, J. Mol. Liq. 342, 117407 (2021); https://doi.org/10.1016/j.molliq.2021.117407.

[21]  N. Danyliuk, T. Tatarchuk, I. Mironyuk, V. Kotsyubynsky, V. Mandzyuk, *Performance of commercial titanium dioxide samples in terms of dye photodegradation assessed using smartphone-based measurements*, Phys. Chem. Solid State., 3, 582 (2022); https://doi.org/10.15330/pcss.23.3.582-589.

[22]  S. Yamasaki, T. Yamada, H. Kobayashi, H. Kitagawa, *Preparation of Sub-10 nm AgI Nanoparticles and a Study on their Phase Transition Temperature*, 73 (2013); https://doi.org/10.1002/asia.201200790.

[23]  K. Ullah, A. Ullah, A. Aldalbahi, J. Do Chung, W.C. Oh, *Enhanced visible light photocatalytic activity and hydrogen evolution through novel heterostructure AgI-FG-TiO₂ nanocomposites*, J. Mol. Catal. A Chem. 410, 242 (2015); https://doi.org/10.1016/j.molcata.2015.09.024.

[24]  W. Liu, C. Wei, G. Wang, X. Cao, Y. Tan, S. Hu, *In situ synthesis of plasmonic Ag@AgI/TiO₂ nanocomposites with enhanced visible photocatalytic performance*, Ceram. Int. 45, 17884 (2019); https://doi.org/10.1016/j.ceramint.2019.06.004.

[25]  A. Shoja, A. Habibi-yangjeh, M. Mousavi, S. Vadivel, *Preparation of novel ternary TiO₂QDs/CDs/AgI nanocomposites with superior visible-light induced photocatalytic activity*, J. Photochem. Photobiol. A Chem. 385, 112070 (2019); https://doi.org/10.1016/j.jphotochem.2019.112070.

[26]  E. Liu, Y. Zhang, Y. Cong, *Highly enhanced photocatalytic reduction of Cr (VI) on AgI/TiO₂ under visible light irradiation: influence of heat pretreatment*, Elsevier B.V. (2015); https://doi.org/10.1016/j.jhazmat.2015.12.050.

[27]  Q.W. Ying-Ying Shao, Wei-Dong Ye, Chun-Yan Sun, Chu-Lin Liu, *Visible-light-induced degradation of polybrominated diphenyl ethers with AgI–TiO₂*, RSC Adv. 7, 39089 (2017); https://doi.org/10.1039/C7RA07106J.

[28] I. Mironyuk, N. Danyliuk, L. Turovska, I. Mykytyn, *Structural, morphological and photocatalytic properties of TiO2 obtained by thermolytic decomposition of the [Ti(OH₂)₆]³⁺•3Cl⁻ aquacomplex*, Phys. Chem. Solid State. 23, 741 (2022); https://doi.org/10.15330/pcss.23.4.741-755.

[29] F. Fazlali, A. Hajian, A. Afkhami, H. Bagheri, *A superficial approach for fabricating unique ternary AgI@TiO₂/Zr-MOF composites: An excellent interfacial with improved photocatalytic light-responsive under visible light,* J. Photochem. Photobiol. A Chem., 112717 (2020); https://doi.org/10.1016/j.jphotochem.2020.112717.

[30] D. Yu, J. Bai, H. Liang, J. Wang, C. Li, Fabrication of a novel visible-light-driven photocatalyst Ag-AgI-TiO₂ nanoparticles supported on carbon *nanofibers*, Appl. Surf. Sci. 349, 241 (2015); https://doi.org/10.1016/j.apsusc.2015.05.019.

[31] D. Wu, M. Long, *Enhancing visible-light activity of the self-cleaning TiO₂-coated cotton fabrics by loading AgI particles*, Surf. Coatings Technol. 206, 1175 (2011); https://doi.org/10.1016/j.surfcoat.2011.08.007.

[32] D. Yu, J. Bai, H. Liang, T. Ma, C. Li, *AgI-modified TiO₂ supported by PAN nanofibers: A heterostructured composite with enhanced visible-light catalytic activity in degrading MO*, Dye. Pigment. 133, 51 (2016); https://doi.org/10.1016/j.dyepig.2016.05.036.

Іван Миронюк[1], Назарій Данилюк[2], Лілія Туровська[3], Ігор Микитин[1], Володимир Коцюбинський[4]

# Структурні, морфологічні та фотокаталітичні властивості наноструктурованого TiO₂/AgI фотокаталізатора

*[1]Кафедра хімії Прикарпатського національний університет імені Василя Стефаника, Івано-Франківськ, Україна, myrif555@gmail*
*[2]Навчально-науковий центр матеріалознавства і нанотехнологій Прикарпатського національного університету імені Василя Стефаника, Івано-Франківськ, Україна, danyliuk.nazariy@gmail.com*
*[3]Кафедра медичної інформатики, медичної та біологічної фізики Івано-Франківського національного медичного університету, Івано-Франківськ, Україна, lturovska@ifnmu.edu.ua*
*[4]Кафедра матеріалознавства та нових технологій Прикарпатського національного університету імені Василя Стефаника, Івано-Франківськ, Україна, kotsuybynsky@gmail.com*

Наноструктурований фотокаталізатор TiO₂/AgI, при дії ультрафіолетового або видимого електромагнітного випромінювання, ефективно знешкоджує у водному середовищі органічні забруднювачі. Він являє собою наноструктуру в якій мікро- та дрібні мезопори анатазного TiO₂ наповнені йодитом срібла в суперіонному стані. Вміст іонопровідної фази α-AgI в об'ємі пор TiO₂ може становити ~ 20 мас.%. Діоксид титану, для одержання фотокаталізатора, синтезують золь-гель методом, використовуючи, як прекурсор розчин титанового аквакомплексу [Ti(OH₂)₆]³⁺•3Cl⁻ та добавку-модифікатор Na₂CO₃. Модифікуюча добавка в процесі синтезу забезпечує вкорінення на поверхні частинок оксидного матеріалу карбонатних групувань =O₂CO. Наявність цих групувань приводить до зростання як об'єму пор так і питомої поверхні TiO₂. Питома поверхня карбонатованого діоксиду титану 368 м²•г⁻¹, об'єм пор 0.28 см³•г⁻¹, а їх розмір 0.9-4.5 нм. Для заповнення мікро- та дрібних мезопор TiO₂ суперіонною α-AgI фазою спочатку на поверхні діоксиду титану з розчину AgNO₃ адсорбують катіони Ag⁺, а після цього здійснюють контактування оксидного матеріалу з розчином KI. Створений наноструктурований фотокаталізатор TiO₂/AgI в порівнянні з фотокаталізатором концерну Evonik марки Р25-TiO₂ демонструє суттєво вищу ефективність щодо фотодеградації органічних барвників Конго червоного та Метилоранжу в видимому та ультрафіолетовому випромінюванні. Найактивніший зразок TiO₂/40AgI досягав повного руйнування барвника КЧ (5 мг/л) за 6 хвилин УФ-опромінення ($\lambda$ = 365 нм), тоді як ефективність комерційного Р25-TiO₂ становила всього 42%, за цей самий проміжок часу.

**Ключові слова:** титан (IV) оксид; Конго червоний; Метилоранж; фотокаталізатор.